The kinematics of late type stars in the solar cylinder studied with SDSS data

Burkhard Fuchs[1], Christian Dettbarn[1], Hans-Walter Rix[2], Timothy C. Beers[3], Dmitry Bizyaev[4], Howard Brewington[4], Hartmut Jahreiß[1], Rainer Klement[2], Elena Malanushenko[4], Viktor Malanushenko[4], Dan Oravetz[4], Kaike Pan[4], Audrey Simmons[4], Stephanie Snedden[4]

ABSTRACT

We study the velocity distribution of Milky Way disk stars in a kiloparsec-sized region around the Sun, based on ~ 2 million M-type stars from DR7 of SDSS, which have newly re-calibrated absolute proper motions from combining SDSS positions with the USNO-B catalogue. We estimate photometric distances to all stars, accurate to $\sim 20\%$, and combine them with the proper motions to derive tangential velocities for this kinematically unbiased sample of stars. Based on a statistical de-projection method we then derive the vertical profiles (to heights of $Z = 800$ pc above the disk plane) for the first and second moments of the three dimensional stellar velocity distribution. We find that $\langle W \rangle = -7 \pm 1$ km/s and $\langle U \rangle = -9 \pm 1$ km/s, independent of height above the mid-plane, reflecting the Sun's motion with respect to the local standard of rest. In contrast, $\langle V \rangle$ changes distinctly from -20 ± 2 km/s in the mid-plane to $\langle V \rangle = -32$ km/s at $Z = 800$ pc, reflecting an asymmetric drift of the stellar mean velocity that increases with height. All three components of the M-star velocity dispersion show a strong linear rise away from the mid-plane, most notably σ_{ZZ}, which grows from 18 km/s ($Z = 0$) to 40 km/s (at $Z = 800$ pc). We determine the orientation of the velocity ellipsoid, and find a significant vertex deviation of 20 to 25 degrees, which decreases only slightly to heights of $Z = 800$ pc. Away from the mid-plane, our sample exhibits a remarkably large tilt of the velocity ellipsoid towards the Galactic plane, which reaches 20° at $Z = 800$ pc and which is not easily explained. Finally, we determine the ratio $\sigma^2_{\phi\phi}/\sigma^2_{RR}$ near the mid-plane, which in the epicyclic approximation implies an almost perfectly flat rotation curve at the Solar radius.

Subject headings: Galaxy: kinematics and dynamics, (Galaxy:) solar neighbourhood

1. Introduction

The velocity distribution of stars in the Milky Way has been most comprehensively studied in the solar vicinity. One of the most long standing systematic collection of relevant data is the *Catalogue of Nearby Stars* (Gliese 1957), with a fourth edition (*CNS4*) now nearly completed (Jahreiß, in preparation). The *CNS4* contains space velocity data for a few thousand stars. A much larger data set, based on stars with proper motions measured by the *Hipparcos* satellite (ESA 1997), was analyzed by Dehnen & Binney (1998). From the proper motions of $\sim 10^4$ stars they could reconstruct the first and second moments of the velocity distribution using a statistical de-projection method which makes use of the many viewing di-

[1]Astronomisches Rechen-Institut am Zentrum für Astronomie der Universität Heidelberg, 69120 Heidelberg, Germany

[2]Max-Planck-Institut für Astronomie, 69117 Heidelberg, Germany

[3]Department of Physics and Astronomy, CSCE: Center for the Study of Cosmic Evolution, and JINA: Joint Institute for Nuclear Astrophysics, Michigan State University, E. Lansing, MI 48824, USA

[4] Apache Point Observatory, Sunspot, NM, 88349, USA

rections through the velocity distribution of the stars. The velocity dispersions of stars in the solar vicinity were also studied by Nordström et al. (2004) from the *Geneva-Copenhagen Survey* of F and G stars. These authors complemented the parallaxes and proper motions of the stars in the *Hipparcos* catalogue by their own radial velocity measurements. With the advent of the deep, wide-field *SDSS* and *RAVE* surveys it has become possible to study the kinematics of stars in the Galactic disk at much larger distances from the Sun. Recently Bochanski et al. (2007) have drawn from the *Fifth Data Release of the Sloan Digitized Sky Survey* (Adelman-McCarthy et al. 2007) a sample of about 7000 K and M stars for which three-dimensional space velocities are available (the SLoMaSS sample). These stars were selected along a line-of-sight which reaches a distance of 1 kpc above the Galactic midplane. Veltz et al. (2008) and Klement et al. (2008) have analyzed the *First Data Release of the RAVE Survey* (Steinmetz et al. 2006). Veltz et al. (2008) inferred the kinematics of stars in the solar cylinder by modeling the distribution of stars in phase space, which was then constrained by star counts of the *RAVE* data. Klement et al. (2008) searched for fine structure in local phase space. Most recently, Siebert et al. (2008) have analyzed the velocity distribution of red clump giants at heights between 500 and 1500 pc above the Galactic midplane, using data from the *Second Data Release of the RAVE Survey* (Zwitter et al. 2008).

In this paper we analyze stellar data from the *Seventh Data Release of the Sloan Digital Sky Survey (SDSS)* (Abazajian et al. 2008), which includes imaging taken as part of the *Sloan Extension for Galactic Understanding and Exploration (SEGUE)* program (Yanny et al. 2008), one of three sub-surveys that were part of first extension of the *SDSS*, known as *SDSS-II*. The *SEGUE* program was designed, in part, to obtain *ugriz* imaging of some 3500 square degrees of sky outside of the original *SDSS-I* footprint (Fukugita et al. 1996, Gunn et al. 1998, 2006, York et al. 2000, Hogg et al. 2001, Smith et al. 2002, Stoughton et al. 2002, Abazajian et al. 2003, 2004, 2005, Pier et al. 2003, Ivezić et al. 2004, Adelman-McCarthy et al. 2006, 2007, 2008, Tucker et al. 2006. The regions of sky targeted are primarily at lower Galactic latitudes ($|b| \lesssim 35^\circ$), in order to better sample the disk/halo interface of the Milky Way. *SEGUE* also obtained $R \simeq 2000$ spectroscopy, over the wavelength range $3800 - 9200$ Å, for some 250,000 stars in 200 selected areas over the sky available from Apache Point, New Mexico (Yanny et al. 2008). The spectroscopic candidates are selected on the basis of *ugriz* photometry to populate target categories chosen to explore the nature of the Galactic stellar populations at distances from 0.5 kpc to over 100 kpc from the Sun. The *SEGUE Stellar Parameter Pipeline* (*SSPP*; see Lee et al. 2008a,b, Allende Prieto et al. 2008) obtained estimates of radial velocities, and in particular, the stellar atmospheric parameters, for the targeted stars over wide ranges of effective temperature ($T_{\rm eff}$), surface gravity ($\log g$), and metallicity ([Fe/H]).

Of central importance to the present paper, the *DR-7* catalog contains astrometric and photometric (*ugriz*) data for well over 100 million stars. Many of these have been identified in the *USNO-B* catalog of proper motions (Monet et al. 2003). These measurements have been improved through a re-calibration effort based on *SDSS* data, and provide us with an extensive set of kinematical data (Munn et al. 2004). After correction of a small systematic error in the data reduction procedure (Munn 2007, internal *SDSS* memorandum; note that the *DR-7 CAS* proper motions have been corrected for this error), the absolute accuracy of the proper motions has reached now a few milliarcseconds per year, corresponding to, e.g., $\sim$5 km/s at a distance of 530 pc for $\epsilon_\mu = 2$ mas/year. They are thus superbly suited to study the kinematics of the Galaxy, especially for stars that populate a local volume.

We have extracted information for about 2 million M-type stars in the solar cylinder from the *SDSS DR-7* database; these stars represent a fair sample of an old, relaxed stellar population mostly drawn from the Galactic thin disk. Using a photometric distance estimator we convert the proper motions into tangential velocities. For individual stars, tangential velocities alone do not allow the construction of space velocity components because the radial velocities are missing. However, Dehnen & Binney (1998) have shown that, by making use of the many viewing angles through the velocity distribution of stars over a large fraction of the sky, the characteristic moments of the

velocity distribution can be determined in a statistical manner. Following this method, we are able to determine empirically, for the first time with high precision, the first and second moments of the velocity distribution of local stars as a function of height above the Galactic midplane.

Our paper is organized as follows. In §2 we describe the sample selection and our methods for obtaining distances and deriving tangential velocities. In §3 we apply the statistical approach of Dehnen & Binney (1998) to reconstruct the moments of the three-dimensional velocity distribution of stars from their tangential velocities. Our conclusions are summarized in §4.

2. Sample Selection, Distance Estimates, and Tangential Velocities

In order to obtain a sample of stars that are representative of the old, relaxed population dominated by the thin disk of the Milky Way, we have extracted from the *SDSS DR-7* database all objects classified as stars in the *de-reddened* color range $0.49 \leq r-i \leq 1.6$, $1.25 < g-r < 1.50$, and with apparent magnitudes $15 < g < 20.5$ (cf. Ivezić et al. 2005). These stars have spectral types M0 and later. The upper cutoff at $g = 20.5$ mag, which corresponds to $r = 19.5$ mag, is necessary because the proper motions are seriously contaminated by misidentifications at fainter magnitudes (Lepine 2008, internal SDSS memorandum). We have selected only stars with non-zero proper motion errors, apparent magnitude errors ≤ 0.05 mag in the g, r, i bands, and which were not flagged for any known astrometric or photometric peculiarities. This resulted in a sample of about 2.6 million stars (mean age expected to be $\sim$5 Gyr).

We have determined a photometric distance estimate for each star using the absolute magnitude-color relations of Jurić et al. (2008). We have compared both the 'faint' and 'bright' normalizations with color-magnitude relations by Davenport et al. (2006) and West et al. (2005). Davenport et al. (2006) have observed M stars drawn from the *Catalogue of Nearby Stars* (Jahreiß & Wielen 1997), for which trigonometric parallaxes are available, in the *ugriz* filter system. West et al. (2005) have selected M dwarfs from the *Third Data Release of the Sloan Digital Sky Survey* (Abazajian et al. 2005) and determined spectroscopic parallaxes of these stars. If we use fits to the West et al. (2005) or Davenport et al. (2006) data as distance estimators in the de-projection formalism (described below) to obtain the first and second moments of the velocity distribution of the stars, we find that the results are practically indistinguishable from the results based on the Jurić et al. (2008) bright normalization. We conclude that this normalization is thus well suited to serve as a photometric distance estimator for red main sequence stars in the Galactic thin disk, such as M dwarfs,

$$\begin{aligned} M_r &= 3.2 + 13.30\,(r-i) - 11.50\,(r-i)^2 \\ &\quad +5.40\,(r-i)^3 - 0.70\,(r-i)^4\,. \end{aligned} \qquad (1)$$

As explained below, we count M dwarfs up to distances reaching 800 pc above the Galactic midplane. According to the model of the Galactic thin and thick disks by Jurić et al. (2008), we expect about 13% of the M dwarfs close to the midplane to be thick-disk stars; in the distance range of 600 to 800 pc above the midplane the fraction of thick disk stars, which are more metal-poor than thin disk stars, is expected to be about 36%. Therefore, we have compared the faint and bright normalizations of Jurić et al. (2008) with the fiducial line delineating the main sequence of the globular cluster M71 as observed by Clem et al. (2008), transformed into the native *ugriz* system using the relations of Tucker et al. (2006), and assuming a distance modulus of $(m-M)_0 = 13.02$. M71 has a metallicity of $[Fe/H]$ = -0.73 (Harris 1996) which is typical for the majority of thick-disk stars. This comparison shows that for metal-poor stars in the color range $r-i > 0.5$, photometric distances can be reliably determined using the faint normalization,

$$\begin{aligned} M_r &= 4.0 + 11.86\,(r-i) - 10.74\,(r-i)^2 \\ &\quad +5.99\,(r-i)^3 - 1.20\,(r-i)^4\,. \end{aligned} \qquad (2)$$

In the following we provide results using both distance scales in order to demonstrate how (little) our results are systematically affected by the presence of thick-disk stars. The difference between the two calibrations is illustrated in Fig. 1 as function of de-reddened $(r-i)_0$ color.

The right ascension and declination, taken together with the distance estimate, were used to

calculate the position of each star in a Cartesian reference system centered on the position of the Sun, with the X-axis pointing toward the Galactic center, the Y-axis in the direction of Galactic rotation, and the Z-axis towards the Galactic north pole, respectively. We then defined eight pill-box shaped counting volumes, oriented parallel to the Galactic midplane and stacked onto each other. Each volume has a vertical height of 100 pc and a radial size $\sqrt{X^2+Y^2} \leq 1$ kpc. The midpoints of the counting volumes are centered on the Galactocentric radius of the Sun and Z = 50, 150, ... 750 pc, respectively. In Fig. 1 we have overlaid frequency distributions of the colors of stars in the distance bin closest to the Galactic midplane and in the most distant bin, respectively, on the absolute magnitude differences between the faint and bright calibrations. These indicate which color ranges of the calibration of the absolute magnitudes are relevant in the various distance bins.

Fig. 2 shows the frequency distributions of the proper motions in right ascension and declination for the stars in each counting volume. Averaged over the entire sample the errors of the proper motions are ϵ_{μ_α} and ϵ_{μ_δ} = 3.36 mas/year.

Fig. 3 illustrates our data as a Hess diagram of the reduced proper motions for our stars

$$H_r = r + 5\,\log\mu + 5 \qquad (3)$$

versus their $(r-i)_0$ colors. In eq. 3 μ denotes the total proper motion of each star in units of mas/year. Even though the stars have been selected into the counting volumes according to their estimated distances, their reduced proper motions are to first order distance independent (Luyten 1939), and are thus also independent from the chosen distance scale. Since M giants are intrinsically brighter (by at least 9 magnitudes) than M dwarfs, they would show up in Fig. 3 in the lower flank of the distribution. As can be seen from Fig. 3, the contamination of our sample by such halo M giants is, as expected (Covey et al. 2008), negligible.

Fig. 4 shows the distribution of the selected stars as function of height above the Galactic midplane versus their $(r-i)_0$ colors. As can be seen in this figure, our sample is volume limited for stars bluer than $(r-i)_0 \leq 0.95$ (with the exception of perhaps a few bright, very nearby stars). In the upper right portion of Fig. 4, red M stars are missing whose apparent magnitudes are fainter than the magnitude limit of the survey.

Returning to Fig. 3, we note a mild Malmquist bias in our sample. The high altitude counting volumes are populated by comparatively more blue stars than red stars, and, given the apparent magnitude limits of the survey, the blue stars are on the average intrinsically brighter.

For each star we have calculated its tangential velocity from the proper motions and the photometric distances based on the bright normalization by Jurić et al. (2008). Assuming zero line-of-sight velocities, we then computed three- dimensional space velocities. Following the notation of Dehnen & Binney (1998), these are referred to as the proper motion velocities p_U, p_V, and p_W. The velocity components are oriented in the same way as the spatial coordinates. Finally, we rejected stars which had at least one single velocity component $>$ 150 km/s. After application of this cut, our final sample comprises 1 898 598 stars. Their spatial distribution is shown in Fig. 5. The errors of the space velocity components were determined by application of a standard Gaussian error propagation formalism. Following Jurić et al. (2008), we have assumed individual relative distance errors of 20%, which corresponds to an error in the absolute magnitudes of 0.43 mag. These errors result in typical errors for the individual velocities of ϵ_{p_U}, ϵ_{p_V}, and ϵ_{p_W} = 2.5(+2, -1) km/s, 2.5(+3, -1) km/s, and 1.5(+3,-1) km/s respectively, but with tails out to $\sim$ 10 km/s. However, the individual errors are greatly diminished when one considers the large number of stars in each of our counting volumes. For instance, if we were to change the individual distance errors from 20 percent to 30 percent, the resulting first and second moments of the velocity distribution would be precisely the same as given in Table 1.

The last step in the preparation of the data was the correction of each individual proper motion velocity for Galactic mean rotation

$$\begin{aligned} p_U &= p_U - (A-B)\,d\cos(b)\sin(l) \\ p_V &= p_V - (A+B)\,d\cos(b)\cos(l), \end{aligned} \qquad (4)$$

where d denotes the distance of a star and l and b are Galactic longitude and latitude, respectively. In this way we have constructed proper motion velocities that reflect the true peculiar velocities of the stars. For the Oort constants A and B we adopt the values determined by

Feast & Whitelock (1997), $A = 14.82$ km/s/kpc and $B = -12.37$ km/s/kpc.

3. Determination of the Velocity Distribution Moments

3.1. Projection Formalism

The proper motion velocities, which we have introduced in the previous section, are formally defined as

$$\begin{pmatrix} p_U \\ p_V \\ p_W \end{pmatrix} = \begin{pmatrix} U \\ V \\ W \end{pmatrix} - ((U,V,W),\vec{e}_r)\ \vec{e}_r, \quad (5)$$

where $\vec{e}_r$ is the unit vector pointing to the star under consideration,

$$\vec{e}_r = \begin{pmatrix} \cos(b)\cos(l) \\ \cos(b)\sin(l) \\ \sin(b) \end{pmatrix}. \quad (6)$$

Equation 5 can be written as a set of algebraic equations

$$\begin{pmatrix} p_U \\ p_V \\ p_W \end{pmatrix} = \mathcal{A} \cdot \begin{pmatrix} U \\ V \\ W \end{pmatrix}. \quad (7)$$

The elements of the symmetric matrix $\mathcal{A}$ are given in Appendix A. The key assumption of the deprojection of the proper motion velocities is that the lines of sight towards the stars are statistically uncorrelated with the velocities of the stars (Dehnen & Binney 1998). We thus take the statistical average of eq. 7 over the samples in each counting volume, as defined above ($\frac{1}{N}\sum_{n=1}^{N}$)

$$\left\langle \begin{pmatrix} p_U \\ p_V \\ p_W \end{pmatrix} \right\rangle = \langle\mathcal{A}\rangle \cdot \left\langle \begin{pmatrix} U \\ V \\ W \end{pmatrix} \right\rangle. \quad (8)$$

In contrast to eq. 7, which cannot be inverted, eq. 8 can be inverted as

$$\left\langle \begin{pmatrix} U \\ V \\ W \end{pmatrix} \right\rangle = \langle\mathcal{A}\rangle^{-1} \cdot \left\langle \begin{pmatrix} p_U \\ p_V \\ p_W \end{pmatrix} \right\rangle, \quad (9)$$

which gives the three first moments of the velocity distribution. Since we presume to have selected a sample from a relaxed population of stars in the Galactic disk, $\langle U\rangle$ and $\langle W\rangle$ should reflect simply the solar motion relative to the standard of the rest, $U_\odot = -\langle U\rangle$ and $W_\odot = -\langle W\rangle$. The quantity $\langle V\rangle$ is, due to the asymmetry of the V velocity distribution, more negative than $-V_\odot$.

Next we consider the second moments of the velocity distribution. The components of the proper motion velocity of each star can be combined as

$$\begin{aligned} p_i p_j &= \sum_{k,m} \mathcal{A}_{ik}\upsilon_k\mathcal{A}_{jm}\upsilon_m \quad (10)\\ &= \frac{1}{2}\sum_{k,m}(\mathcal{A}_{ik}\mathcal{A}_{jm} + \mathcal{A}_{jk}\mathcal{A}_{im})\upsilon_k\upsilon_m, \end{aligned}$$

where the indices stand for $i,j,k,m = U,V,W$ and $(\upsilon_U,\upsilon_V,\upsilon_W) = (U,V,W)$. Again we take the ensemble average

$$\langle p_i p_j\rangle = \frac{1}{2}\sum_{k,m}\langle\mathcal{A}_{ik}\mathcal{A}_{jm} + \mathcal{A}_{jk}\mathcal{A}_{im}\rangle\langle\upsilon_k\upsilon_m\rangle, \quad (11)$$

which is manifestly symmetric in the indices i,j. Formally, we set up a set of algebraic equations

$$\left\langle \begin{matrix} p_Up_U \\ p_Up_V \\ p_Up_W \\ p_Vp_V \\ p_Vp_W \\ p_Wp_W \end{matrix} \right\rangle = \langle\mathcal{B}\rangle \cdot \left\langle \begin{matrix} UU \\ UV \\ UW \\ VV \\ VW \\ WW \end{matrix} \right\rangle, \quad (12)$$

Since the lines of sight to the stars are statistically uncorrelated with their velocities, the matrix $\langle\mathcal{B}\rangle$ is also not singular, and allows for each Z-slice the inversion

$$\left\langle \begin{matrix} UU \\ UV \\ UW \\ VV \\ VW \\ WW \end{matrix} \right\rangle = \langle\mathcal{B}\rangle^{-1} \cdot \left\langle \begin{matrix} p_Up_U \\ p_Up_V \\ p_Up_W \\ p_Vp_V \\ p_Vp_W \\ p_Wp_W \end{matrix} \right\rangle. \quad (13)$$

The elements of matrix $\mathcal{B}$ are also given in Appendix A.

The velocity dispersions are given by $\sigma^2_{RR} = \langle UU\rangle - \langle U\rangle^2$, $\sigma^2_{\phi\phi} = \langle VV\rangle - \langle V\rangle^2$, $\sigma^2_{ZZ} = \langle WW\rangle - \langle W\rangle^2$ and we have the mixed moments $\sigma^2_{R\phi} = -(\langle UV\rangle - \langle U\rangle\langle V\rangle)$, $\sigma^2_{RZ} = -(\langle UW\rangle - \langle U\rangle\langle W\rangle)$, $\sigma^2_{\phi Z} = \langle VW\rangle - \langle V\rangle\langle W\rangle$. In the definition of the latter, we have switched from U to $\dot{R} = -U$ which is, for instance, more convenient to use with the Jeans equations.

It seems intuitive that this inversion should work for an all-sky sample, but less so in the case of the *SDSS* coverage. In order to test that the sky coverage of the selected sample of stars is sufficient to reliably invert eqns. 8 and 12, we have carried out a Monte-Carlo simulation. We have assigned to each star in the counting volumes a space velocity drawn randomly from the Schwarzschild distribution

$$f \propto \exp -\frac{1}{2}\left[\left(\frac{U-\langle U\rangle}{\sigma_{RR}}\right)^2 + \left(\frac{V-\langle V\rangle}{\sigma_{\phi\phi}}\right)^2 + \left(\frac{W-\langle W\rangle}{\sigma_{ZZ}}\right)^2\right] \quad (14)$$

with $\langle U\rangle$ = -10 km/s, $\langle V\rangle$ = -26 km/s, $\langle W\rangle$ = -7 km/s, $\sigma_{RR} = 45$ km/s, $\sigma_{\phi\phi} = 32$ km/s, and $\sigma_{ZZ} = 24$ km/s. We have converted the space velocities to proper motion velocities and found that we could reconstruct, from just the samples contained in the *SDSS* footprint, both the assumed velocity offsets and velocity dispersions to accuracies of 0.2 km/s, respectively.

3.2. Results

The de-projection procedure provides us with an observational estimate of the stellar velocity dispersion ellipsoid as a function of height above the Galactic midplane. Results are given in Table 1 and illustrated in Fig. 6. The error calculus for all entries in the table is described in Appendix B. As can be seen in Fig. 6, there is a mild scatter of the data points which we ascribe to individual distance errors.

In order to demonstrate the systematic effect of the adopted distance scale, we also show in Fig. 6 kinematical results based on the faint normalization of the main sequence by Jurić et al. (2008). As discussed in §2, this distance scale is appropriate for metal-poor thick-disk stars. Since our sample is presumed to be significantly contaminated by thick-disk stars only in the most distant counting volumes, the alternative distance scale should be actually used only in these counting volumes. As can be seen from the panels on the right hand side of Fig. 6, switching the distance scale leads to differences of the the mean motions and velocity dispersions of 1 to 2 km/s, with the exception of σ_{RR}, which deviates by up to 3 km/s. These changes are unexpectedly small, but can be understood from closer inspection of Fig. 1. The lowest distance bin is populated by comparatively red stars with typical colors $1.1 \lesssim (r-i)_0 \lesssim$ <1.5. As can be seen from Fig. 1, the difference M_r(faint) − M_r(bright) ranges in this color range from 0.2 to -0.2, mag so that in the statistical average no change of the kinematic results is expected. In the most distant bin, $0.5 < (r-i)_0 < 1$, the difference M_r(faint) − M_r(bright) is about 0.2 mag, which corresponds to a distance scale contraction of 9%. However, as a result of the reduced distance estimates, stars will wander into the Z-slice from above, and some stars will drop through the bottom of the counting volume. As can be seen from Fig. 4, the incoming stars (from above) will be systematically bluer than the stars which they replace (from below). The former will also be systematically brighter, which compensates to a considerable degree the switch from the bright to the faint calibration of the absolute magnitudes. Thus, the systematic errors of the kinematical data introduced by systematic errors in the distance scale are only of order $\sim$ 1 to 2 km/s.

As an independent consistency check on our results, we have retrieved from the SpecPhoto database of *SDSS DR-7* the radial velocities of all stars at galactic latitudes $b \geq 70°$ in the color window $1.0 \leq g-r \leq 1.5$ and $0.3 \leq r-i \leq 1.6$. Since these stars lie close to the Galactic pole, their radial velocities reflect their W velocity components. The resulting mean velocities and velocity dispersions are summarized as a function of height above the Galactic midplane in Table 2. As can be seen from a comparison with Table 1, the vertical velocity dispersions determined in this way are in excellent agreement with those estimated from proper motions alone.

The second row in Table 1 lists, for comparison, kinematical data for late-type stars[1] reproduced from the *CNS4* (Jahreiß, in preparation), which contains data for stars within a distance of 25 pc from the Sun. With the exception of the mean radial velocity $\langle U\rangle$, the other first and second moments of the velocity distribution determined in the Z = 0-100 pc sample of *SDSS* stars are remarkably consistent with the relatively tiny sample of nearby stars. The third row in Ta-

[1] Groups 2-5 as defined in Jahreiß & Wielen (1997)

TABLE 1

FIRST AND SECOND MOMENTS OF THE VELOCITY DISTRIBUTION AS FUNCTION OF HEIGHT ABOVE THE GALACTIC MIDPLANE

Z *pc*	N	$\langle U \rangle$ km/s	$\langle V \rangle$ km/s	$\langle W \rangle$ km/s	σ_{RR} km/s	$\sigma_{\phi\phi}$ km/s	σ_{ZZ} km/s	$\langle UV \rangle$ $(km/s)^2$	$\langle UW \rangle$ $(km/s)^2$	$\langle VW \rangle$ $(km/s)^2$
0–100	48 075	-8.62	-20.04	-7.10	32.4	23.0	18.1	320.7	32.1	127.4
		0.22	0.14	0.16	0.11	0.09	0.18	3.9	3.7	2.3
CNS4	*600*	*-12.2*	*-22.3*	*-6.9*	*38.2*	*25.6*	*19.4*	151.1	-26.7	-1.8
		2.1	*1.5*	*1.3*	*1.7*	*1.4*	*1.3*	-	-	-
DB98	*∼ 1 300*	*-10.44*	*-24.59*	*-8.17*	*36.8*	*26.7*	*18.3*	*416.0*	*-86.1*	*202.7*
		1.69	*1.71*	*1.78*	*1.18*	*1.72*	*2.58*	-	-	-
100–200	280 929	-8.10	-21.62	-7.14	35.3	24.9	20.9	298.9	7.1	143.3
		0.09	0.06	0.08	0.04	0.04	0.08	1.7	1.7	1.2
200–300	387 749	-8.05	-22.37	-7.49	38.5	27.2	24.9	292.9	-42.2	149.6
		0.08	0.05	0.08	0.04	0.03	0.08	1.6	1.7	1.4
300–400	360 829	-9.06	-23.51	-7.29	41.5	29.8	28.0	325.5	-75.9	137.0
		0.08	0.06	0.09	0.04	0.04	0.10	1.9	2.1	1.9
400–500	302 601	-9.62	-24.76	-7.35	43.1	31.7	30.6	332.2	-125.4	135.6
		0.09	0.07	0.11	0.05	0.05	0.13	2.3	2.7	2.5
500–600	237 746	-10.28	-26.22	-7.12	45.0	33.6	33.3	342.8	-181.1	122.3
		0.11	0.09	0.14	0.06	0.06	0.17	3.0	3.6	3.6
600–700	168 595	-10.19	-28.61	-7.12	47.0	35.4	36.6	358.6	-232.5	132.3
		0.13	0.11	0.19	0.08	0.07	0.23	3.9	4.7	5.0
700–800	112 074	-10.42	-32.18	-7.18	49.1	37.6	40.0	419.2	-263.0	166.8
		0.17	0.14	0.27	0.11	0.09	0.36	5.4	6.9	7.7

Col. (1): distance interval, col. (2): number of stars, cols. (3) to (5): mean velocity components and their errors (below), cols. (6) to (8): velocity dispersions and their errors (below), cols. (9) to (11): mixed moments of the velocity ellipsoid and their errors (below). The errors represent only internal errors. Systematic errors can be as large as 2-3 km/s.

TABLE 2

FIRST AND SECOND MOMENTS OF THE DISTRIBUTION OF SPECTROSCOPICALLY MEASURED LINE-OF-SIGHT VELOCITIES[†] OF M DWARFS AT LATITUDES $b \geq 70°$

Z pc	N	$\langle V_{los} \rangle$ km/s	$\epsilon_{\langle V_{los} \rangle}$ km/s	$\sigma_{V_{los}}$ km/s	$\epsilon_{\sigma_{V_{los}}}$ km/s
0–200	272	-9.5	0.6	24.0	1.0
200–400	770	-12.0	0.4	27.6	0.7
400–600	247	-8.5	0.5	29.7	1.3
600–800	64	-16.0	2.0	39.6	3.5

[†]SpecPhoto data from *SDSS DR-7*

ble 1 gives the results of Dehnen & Binney (1998) in their reddest bin, which corresponds to K-type stars. Again, there is good agreement between their results and the results in our low latitude sample. We note as well that Veltz et al. (2008) find, from their analysis of the *RAVE* survey (Steinmetz et al. 2006) $\langle U \rangle$ = -8.5 km/s, which is very close to our SDSS result. Moreover, we can compare our results with the observations of the SLoMaSS stars by Bochanski et al. (2007). For this purpose we have combined all 1 380 183 stars with $0 < Z < 500$ pc and derived with the statistical de-projection method velocity dispersions $(\sigma_{RR}, \sigma_{\phi\phi}, \sigma_{ZZ})$ = (40.0, 28.5, 25.4) km/s. These are in excellent agreement with the measurements by Bochanski et al. (2007) (39.0, 30.0, 24.8) km/s.

The distribution of the U-velocity components of the stars is expected to be symmetrical with respect to the local standard of rest (LSR). Thus the mean velocity $\langle U \rangle$ reflects the solar motion relative to the LSR, $\langle U \rangle = -U_{\odot}$. But as can be seen from Table 1, we find a slight, but statistically significant, decrease of $\langle U \rangle$ with increasing height above the midplane. This might indicate some radially inward streaming of the local stars relative to the rest of the disk, perhaps induced by a spiral arm.

The mean rotation velocity $\langle V \rangle$ does not simply reflect the solar motion $-V_{\odot}$, but is much more negative due to the asymmetrical shape of the distribution of the V-velocity components of the stars. The solar motion in V alone would be reflected by a subsample of young stars with very small velocity dispersions (cf. Dehnen & Binney 1998), which we cannot isolate in our data, because we do not know the individual space velocities of the stars. The fourth column of Table 1 shows that the mean rotation velocity of stars slows down systematically with height above the midplane, as $\Delta\langle V \rangle / \Delta\sigma^2_{RR}$ = -0.0089 $(\mathrm{km/s})^{-1}$, and $\Delta\langle V \rangle / \Delta Z$ = - 0.017 km/s/kpc. The latter is expected due to the asymmetric drift effect (Binney & Tremaine 1987). A quantitative interpretation of this effect is not possible on the basis of the present data. For Jeans modeling of the Milky Way disk, the radial gradient of the σ_{RR} velocity dispersion must be known. Unfortunately, this cannot be measured using stars from the *SDSS DR-7* sample, but we hope to address this problem in the near future.

The quantity $\langle W \rangle = -W_{\odot}$ stays constant with height above the midplane.

The velocity dispersions σ_{RR}, $\sigma_{\phi\phi}$, and σ_{ZZ} rise systematically with height above the midplane, Z. This rise is expected due to two effects. Even the relaxed population of M-type stars represents an age mix of young and old stars. Since the work of Spitzer & Schwarzschild (1951), it is well known that older stars exhibit, as a result of 'disk heating', significantly larger velocity dispersions than younger stars (see Fuchs et al. 2001 for a review). Stars with larger vertical σ_{ZZ} velocity dispersions can ascend higher into the Galactic gravitational potential, so that one expects to find stars with higher velocity dispersions at greater heights above the midplane than closer to the midplane (Fuchs & Wielen 1987, West et al. 2008). Furthermore, our sample transitions with increasing height above the midplane from the old thin-disk to the thick- disk population. Thick-disk stars have velocity dispersions on the order of $(\sigma_{RR}, \sigma_{\phi\phi}, \sigma_{ZZ})$ = (45-65, 40-50, 30-40) km/s (Chiba & Beers 2000, Alcobé & Cubarsi 2005, Holmberg et al. 2007), which are only slightly larger than what we actually measure. We have estimated, from the 50% contour level of the velocity distribution of red clump giants at altitudes between 500 pc and 1500 pc above the midplane derived by Siebert et al. (2008) with *RAVE DR-2* data, velocity dispersions of about $(\sigma_{RR}, \sigma_{\phi\phi}, \sigma_{ZZ}) \approx$ (79, 56, 35) km/s. The vertical velocity dispersion is consistent with our measurement in the highest altitude bin, whereas the planar velocity dispersions are significantly higher than our measurements, and, particularly in the U velocity component, even higher than what is commonly ascribed to thick-disk stars. We note, however, that such high σ_{RR} and $\sigma_{\phi\phi}$ dispersions are comparable with the velocity dispersions ascribed by Bochanski et al. (2007) to the high-dispersion wings of the velocity distribution of the stars in their sample. Thus, the sample of Siebert et al. (2008), with a 'ceiling' at Z = 1500 pc, seems to be contaminated by hot metal-weak thick disk (Chiba & Beers 2000) and halo stars; the tilt of the velocity ellipsoid which they measure might not reflect that of disk stars.

The rotational lag of the stars is tied by the asymmetric drift effect to the radial velocity dispersion σ_{RR}, so that $-\langle V \rangle$ increases with Z, pre-

cisely as observed. As explained above, a quantitative modeling of this effect is not possible on the basis of the present data alone.

Owing to the richness of our data, we were able to split them up into subsets based on color. As a test, we have selected only those stars with colors in the range $0.49 \leq (r-i)_0 \leq 0.95$, where our sample is volume complete (cf. Fig. 4). If we use only these stars in the de-projection of the proper motion velocities, we find the first and second moments of the velocity distribution illustrated in Fig. 7. A comparison with Fig. 6 shows that the kinematical results inferred from the 'blue' subset are entirely consistent with that of the total data set. Only in the $\langle V \rangle$ velocity component do we find, close to the midplane, an offset of 4 km/s.

Next we discuss the off-diagonal elements of the velocity dispersion tensor. The mixed moment $\sigma_{R\phi}$ is illustrated in Fig. 8 as a function of height above the Galactic midplane. The inset of Fig. 8 shows the implied vertex deviation

$$\psi = -\frac{1}{2} \arctan \frac{2\,\sigma^2_{R\phi}}{\sigma^2_{RR} - \sigma^2_{\phi\phi}}\,. \qquad (15)$$

As can be seen from Fig. 8, the vertex deviation is non-negligible, even if it falls slightly with height above the midplane. Close to the midplane our measurement is consistent with the result of Dehnen & Binney (1998). Since our sample of stars is supposed to be drawn from a dynamically relaxed population of the Milky Way, the vertex deviation is almost certainly due to dynamical effects induced by non-axisymmetric structures in the Galactic disk.

The moment σ^2_{RZ} can be used to determine the apparent tilting angle of the velocity ellipsoid in the meridional plane spanned by U and W,

$$\alpha = -\frac{1}{2} \arctan \frac{2\,\sigma^2_{RZ}}{\sigma^2_{RR} - \sigma^2_{ZZ}}\,. \qquad (16)$$

The mixed moment itself is shown as $-\sqrt{\sigma^2_{RZ}}$ in Fig. 9 as a function of height above the Galactic midplane. The resulting tilting angle α is depicted in the inset of Fig. 9. Close to the midplane we find $\alpha \approx 0$ implying that the velocity ellipsoid points towards the Galactic Center. Above the midplane the velocity ellipsoid is tilted towards the Galactic center, however, by a much larger angle than previously thought (Binney & Tremaine 1987, Gilmore 1989, Kent & de Zeeuw 1991). At a height of $Z = 750$ pc the velocity ellipsoid is tilted by $\alpha = -20°$, whereas one would expect $\alpha = -5.4°$ if the velocity ellipsoid was pointing straight towards the Galactic center. In order to assess the plausibility of this unexpected result we address each of the three input parameters of eq. 16 in turn. We have already tested above our measurements of the vertical velocity dispersions σ_{ZZ} using a completely different sample of M stars, for which the line-of-sight velocities in the direction towards the Galactic pole are known. The radial velocity dispersions σ_{RR} can be checked in a similar way. We have determined the first and second moments of the distribution of the p_U and p_V proper motion velocity components of those stars in our sample which lie in the cone $b \geq 70°$. In the upper most counting volume, at 700 pc $\leq Z \leq$ 800 pc, we find $\sqrt{\langle p_U p_U \rangle - \langle p_U \rangle^2} = 47.9 \pm 0.2$ km/s and $\sqrt{\langle p_V p_V \rangle - \langle p_V \rangle^2} = 36.1 \pm 0.2$ km/s, which are in excellent agreement with the result of our de-projection formalism (see Table 1). There is no independent test of the mixed moment σ^2_{RZ} within our data at this altitude, but we note that the tilting angle of the velocity ellipsoid of $\alpha = 7.3°$ reported by Siebert et al. (2008) implies $\sigma^2_{RZ} \approx 650$ (km/s)^2, which is even more than what we find. At mid altitudes, around 400 pc above the midplane, the sample of M stars with known radial velocities (described above) provides an independent check on the mixed moment σ^2_{RZ}. We have drawn from the SpecPhoto database of *SDSS DR-7* a set of 201 stars with $b \geq 70°$ at heights of $400 < Z < 600$ pc above the midplane, with a mean of $\langle Z \rangle = 450$ pc. Since the stars lie in the cone $b \geq 70°$, the line-of-sight velocities reflect their W velocity components; we obtain $\sigma_{V_{los}} = 29.2 \pm 0.7$ km/s. From the proper motion velocities p_U we derive $\sqrt{\langle p_U p_U \rangle - \langle p_U \rangle^2} = 46.8 \pm 1.8$ km/s. We have then cross-correlated the V_{los} and p_U velocity components, giving $\langle V_{los} p_U \rangle$ = -275.5 ± 46 (km/s)^2, which implies a tilting angle of $\alpha = 11.2 \pm 1.7$ degrees. If the velocity ellipsoid were pointing towards the Galactic center, one would expect $\alpha =$ 3.2 degrees. A comparison of these independent kinematic data with the seventh and eighth row of Table 1 and Fig. 9 shows excellent agreement with the results from the statistical de-projection of the proper motion velocities. We conclude from this discussion that our measurement of the tilt-

ing angle of the velocity dispersion tensor should be quite robust.

Finally, we determine the epicyclic ratio, which is related to the slope of the Galactic rotation curve as

$$\frac{d\ln v_c}{d\ln r} = 2\,\frac{\sigma^2_{\phi\phi}}{\sigma^2_{RR}} - 1\,, \qquad (17)$$

Close to the midplane, we find a value of $\frac{d\ln v_c}{d\ln r}$ = -0.006 ± 0.016. which indicates a flat Galactic rotation curve in the solar neighborhood. Note, however, that the quoted error reflects only internal errors. Equation (17) neglects the asymmetric shape of the distribution of the V velocity components of the stars. In order to correct for this simplification, third moments of the velocity distribution must be known (Cuddeford & Binney 1994), which we have not measured here.

4. Conclusions

We have analyzed the velocity distribution of stars in the Galactic old thin-disk population using stellar data from the *Seventh Data Release of the Sloan Digital Sky Survey*. We have constructed a sample of about 2 million late-type stars in eight cylindrical counting volumes, each of which has a height of 100 pc and a diameter of 2 kpc, respectively, and which were stacked onto one another. For each star we have determined a photometric distance estimate, and combined this with their available proper motions to obtain tangential velocities. These were then treated as pseudo space velocities. We have demonstrated with Monte Carlo simulations that our sample provides sufficient lines of sight through the velocity distribution of the stars that the pseudo space velocities allow for a precise statistical determination of the first and second moments of the three dimensional velocity distribution. Close to the Galactic midplane we find $\langle U\rangle$ = -8.6 ± 0.2 km/s and $\langle W\rangle$ = -7.1 ± 0.2 km/s, which directly reflect the motion of the sun relative to the Local Standard of Rest. The mean V velocity component, $\langle V\rangle$ = -20.0 ± 0.1 km/s, is much more negative than just the reflex of the solar motion, due to the asymmetric shape of the V velocity distribution. Close to the midplane, we obtain estimates of the velocity dispersions $\sigma_{RR} = 32.4 \pm 0.1$ km/s, $\sigma_{\phi\phi} = 23.0 \pm 0.1$ km/s, and $\sigma_{ZZ} = 18.1 \pm 0.2$ km/s, respectively. With the exception of $\langle U\rangle$, all of these results are consistent with other determinations, such as analyses of the *Catalogue of Nearby Stars* or *Hipparcos* stars by Dehnen & Binney (1998). However, due to the large number of stars we reach an unprecedented precision, up to ten times better than previously achieved. Moreover, we have a sufficient sample to trace all quantities as a function of height above the Galactic midplane. The velocity dispersions exhibit a distinct increase with height above the midplane. This is a clear indication that our sample of M stars contains a mixture of young stars with low velocity dispersions and old stars with high velocity dispersions, because only the latter ascend high above the midplane. Since the rotational lag of the stars is tied by the asymmetric drift effect to the radial velocity dispersion, -$\langle V\rangle$ must increase also with height above the midplane, precisely as observed.

We have then studied the orientation of the velocity ellipsoid in the meridional planes spanned by the U, V, and W velocity components. We find a vertex deviation of the velocity ellipsoid of about 20° to 25°. Close to the Galactic midplane the ellipsoid is oriented parallel to the Galactic plane. At a height of 750 pc above the midplane the velocity ellipsoid is tilted by an angle of about $\alpha = -20°$. This is more than thought previously, because a tilting angle of $\alpha = -5.4°$ is expected at that altitude, if the velocity ellipsoid points straight at the Galactic Center.

Finally, we determined the epicyclic ratio which indicates, close to the midplane, a flat shape of the Galactic rotation curve in the solar neighborhood.

We have refrained in this paper from any detailed dynamical modelling of our data but hope to address this topic in the near future.

Funding for the SDSS and SDSS-II has been provided by the Alfred P. Sloan Foundation, the Participating Institutions, the National Science Foundation, the U.S. Department of Energy, the National Aeronautics and Space Administration, the Japanese Monbukagakusho, the Max Planck Society, and the Higher Education Funding Council for England. The SDSS Web Site is http://www.sdss.org/.

The SDSS is managed by the Astrophysical Research Consortium for the Participating Institutions. The Participating Institutions are the

American Museum of Natural History, Astrophysical Institute Potsdam, University of Basel, University of Cambridge, Case Western Reserve University, University of Chicago, Drexel University, Fermilab, the Institute for Advanced Study, the Japan Participation Group, Johns Hopkins University, the Joint Institute for Nuclear Astrophysics, the Kavli Institute for Particle Astrophysics and Cosmology, the Korean Scientist Group, the Chinese Academy of Sciences (LAMOST), Los Alamos National Laboratory, the Max-Planck-Institute for Astronomy (MPIA), the Max-Planck-Institute for Astrophysics (MPA), New Mexico State University, Ohio State University, University of Pittsburgh, University of Portsmouth, Princeton University, the United States Naval Observatory, and the University of Washington.

Appendix A: The Matrices $\mathcal{A}$ and $\mathcal{B}$

The elements of matrix $\mathcal{A}$ are given by

$$\begin{aligned}
\mathcal{A}_{UU} &= 1-\cos^2(b)\cos^2(l) \\
\mathcal{A}_{UV} &= -\cos^2(b)\cos(l)\sin(l) = \mathcal{A}_{VU} \\
\mathcal{A}_{UW} &= -\sin(b)\cos(b)\cos(l) = \mathcal{A}_{WU} \\
\mathcal{A}_{VV} &= 1-\cos^2(b)\sin^2(l) \\
\mathcal{A}_{VW} &= -\sin(b)\cos(b)\sin(l) = \mathcal{A}_{WV} \\
\mathcal{A}_{WW} &= \cos^2(b)\,. \qquad (18)
\end{aligned}$$

The elements of matrix $\mathcal{B}$ are defined straightforwardly by eq. 11, but are a bit cumbersome to write out explicitely. We consider $\mathcal{B}(nr,nc)$, where nr and nc are the numbers of the rows and columns in the matrix $\mathcal{B}$. Next we introduce two tables of indices $icol$ and $irow$ and write, if nc equal 1, 4, or 6

$$\begin{aligned}
\mathcal{B}(nr,nc) &= \frac{1}{2}\,[\mathcal{A}(irow(nr,1),icol(nc,1)) \\
&\quad *\mathcal{A}(irow(nr,2),icol(nc,2)) \qquad (19) \\
&\quad +\mathcal{A}(irow(nr,3),icol(nc,3)) \\
&\quad *\mathcal{A}(irow(nr,4),icol(nc,4))]\,.
\end{aligned}$$

For the other combinations we have

$$\begin{aligned}
\mathcal{B}(nr,nc) &= \frac{1}{2}\,[\mathcal{A}(irow(nr,1),icol(nc,1)) \\
&\quad *\mathcal{A}(irow(nr,2),icol(nc,2)) \\
&\quad +\mathcal{A}(irow(nr,3),icol(nc,3)) \\
&\quad *\mathcal{A}(irow(nr,4),icol(nc,4)) \qquad (20) \\
&\quad +\mathcal{A}(irow(nr,1),icol(nc,5)) \\
&\quad *\mathcal{A}(irow(nr,2),icol(nc,6)) \\
&\quad +\mathcal{A}(irow(nr,3),icol(nc,7)) \\
&\quad *\mathcal{A}(irow(nr,4),icol(nc,8))]\,.
\end{aligned}$$

The indices $irow$ and $icol$ of matrix $\mathcal{A}$ stand for $irow, icol = 1,2,3, = U,V,W$, respectively.

Appendix B: Error Calculus

We consider first the moments $\langle U\rangle$, $\langle V\rangle$, and $\langle W\rangle$. Each proper motion velocity component has an individual error ϵ_U, ϵ_V, ϵ_W. The error of the statistically averaged proper motion velocity components is given by

$$\epsilon^2_{\langle p_U\rangle,\langle p_V\rangle,\langle p_W\rangle} = \frac{1}{N^2}\sum_{n=1}^{N}\epsilon^2_{p_{U,n},p_{V,n},p_{W,n}}\,, \qquad (21)$$

where N denotes the number of stars in the counting volume. We neglect positional errors so that matrix elements of $\langle\mathcal{A}\rangle$ have no errors. The errors of the first moments of the velocity distribution follow then as

$$\begin{aligned}
\epsilon^2_{\langle U\rangle} = (\langle\mathcal{A}_{UU}\rangle^{-1})^2\epsilon^2_{\langle p_U\rangle} &+ (\langle\mathcal{A}_{UV}\rangle^{-1})^2\epsilon^2_{\langle p_V\rangle} \\
&+(\langle\mathcal{A}_{UW}\rangle^{-1})^2\epsilon^2_{\langle p_W\rangle} \\
\epsilon^2_{\langle V\rangle} = (\langle\mathcal{A}_{VU}{}^{-1}\rangle)^2\epsilon^2_{\langle p_U\rangle} &+ (\langle\mathcal{A}_{VV}{}^{-1}\rangle)^2\epsilon^2_{\langle p_V\rangle} \qquad (22) \\
&+(\langle\mathcal{A}_{VW}\rangle^{-1})^2\epsilon^2_{\langle p_W\rangle} \\
\epsilon^2_{\langle W\rangle} = (\langle\mathcal{A}_{WU}{}^{-1}\rangle)^2\epsilon^2_{\langle p_U\rangle} &+ (\langle\mathcal{A}_{WV}{}^{-1}\rangle)^2\epsilon^2_{\langle p_V\rangle} \\
&+(\langle\mathcal{A}_{WW}\rangle^{-1})^2\epsilon^2_{\langle p_W\rangle}\,.
\end{aligned}$$

The errors of the statistical averages of the combinations of the proper motion velocity components are given by

$$\begin{aligned}
\epsilon^2_{\langle p_U p_U\rangle} &= \frac{4}{N^2}\sum_{n=1}^{N} p^2_{U,n}\epsilon^2_{p_{U,n}} \\
\epsilon^2_{\langle p_U p_V\rangle} &= \frac{1}{N^2}\sum_{n=1}^{N} p^2_{V,n}\epsilon^2_{p_{U,n}} + p^2_{U,n}\epsilon^2_{p_{V,n}} \\
\epsilon^2_{\langle p_U p_W\rangle} &= \frac{1}{N^2}\sum_{n=1}^{N} p^2_{W,n}\epsilon^2_{p_{U,n}} + p^2_{U,n}\epsilon^2_{p_{W,n}} \\
\epsilon^2_{\langle p_V p_V\rangle} &= \frac{4}{N^2}\sum_{n=1}^{N} p^2_{V,n}\epsilon^2_{p_{V,n}} \qquad (23)
\end{aligned}$$

Table 3
Index table irow(nr,j)

nr	j=1	j=2	j=3	j=4
1	1	1	1	1
2	1	2	2	1
3	1	3	3	1
4	2	2	2	2
5	2	3	3	2
6	3	3	3	3

Table 4
Index table icol(nc,j)

nc	j=1	j=2	j=3	j=4	j=5	j=6	j=7	j=8
1	1	1	1	1	-	-	-	-
2	1	2	1	2	2	1	2	1
3	1	3	1	3	3	1	3	1
4	2	2	2	2	-	-	-	-
5	2	3	2	3	3	2	3	2
6	3	3	3	3	-	-	-	-

$$\epsilon^2_{\langle p_V p_W\rangle} = \frac{1}{N^2}\sum_{n=1}^{N} p^2_{W,n}\epsilon^2_{p_{V,n}} + p^2_{V,n}\epsilon^2_{p_{W,n}}$$

$$\epsilon^2_{\langle p_W p_W\rangle} = \frac{4}{N^2}\sum_{n=1}^{N} p^2_{W,n}\epsilon^2_{p_{W,n}}$$

The errors of the second moments of the velocity distribution follow then as

$$\begin{aligned}\epsilon^2_{\langle UU\rangle} &= (\langle\mathcal{B}_{11}\rangle^{-1})^2\epsilon^2_{\langle p_U p_U\rangle} + (\langle\mathcal{B}_{12}\rangle^{-1})^2\epsilon^2_{\langle p_U p_V\rangle} \\ &+ (\langle\mathcal{B}_{13}\rangle^{-1})^2\epsilon^2_{\langle p_U p_W\rangle} + (\langle\mathcal{B}_{14}\rangle^{-1})^2\epsilon^2_{\langle p_V p_V\rangle} \quad (24)\\ &+ (\langle\mathcal{B}_{15}\rangle^{-1})^2\epsilon^2_{\langle p_V p_W\rangle} + (\langle\mathcal{B}_{16}\rangle^{-1})^2\epsilon^2_{\langle p_W p_W\rangle} \\ \epsilon^2_{\langle UV\rangle} &= (\langle\mathcal{B}_{21}\rangle^{-1})^2\epsilon^2_{\langle p_U p_U\rangle} + (\langle\mathcal{B}_{22}\rangle^{-1})^2\epsilon^2_{\langle p_U p_V\rangle} + ...\end{aligned}$$

and so on.

REFERENCES

Abazajian, K., Adelman-McCarthy, J. K., Agüeros, M. A., Allam, S. S., Anderson, S. F. et al. 2003, AJ, 126, 2081

Abazajian, K., Adelman-McCarthy, J. K., Agüeros, M. A., Allam, S. S., Anderson, K. et al. 2004, AJ, 128, 502

Abazajian, K., Adelman-McCarthy, J. K., Agüeros, M. A., Allam, S. S., Anderson, K. S. J. et al. 2005, AJ, 129, 1755

Abazajian, K. N., Adelman-McCarthy, J. K., Agüeros, M. A., Allam, S. S., Allende, C. et al. 2008, (arXiv:0812.0649)

Adelman-McCarthy, J. K., Agüeros, M. A., Allam, S. S., Anderson, K. S. J., Anderson, S. F. et al. 2006, ApJS, 162, 38

Adelman-McCarthy, J. K., Agüeros, M. A., Allam, S. S., Anderson, K. S. J., Anderson, S. F. et al. 2007, ApJS, 172, 634

Adelman-McCarthy, J. K., Agüeros, M. A., Allam, S. S., Allende-Prieto, C., Anderson, K. S. J., et al. 2008, ApJS, 175, 297

Alcobé, S., Cubarsi, R. 2005, A&A, 442, 929

Allende Prieto, C., Sivarani, T., Beers, T. C., Lee, Y. S., Koesterke, L., Shetrone, M., et al. 2008, AJ, 136, 2070

Binney, J., Tremaine, S. 1987, Galactic Dynamics, Princeton: Princeton Univ. Press

Bochanski, J. J., Munn, J. A., Hawley, S. L., West, A. A., Covey, K. R., & Schneider, D. P. 2007, AJ, 134, 2418

Chiba, M., Beers T.C. 2000, AJ, 119, 2843

Clem, J. L., Vanden Berg, D. A., Stetson, P. B. 2008, AJ, 135, 682

Covey, K. R., Hawley, S. L., Bochanski, J. J, West, A. A., Reid, I. N. et al. 2008, AJ, 136, 1778

Cuddeford, P., Binney, J. 1994, MNRAS, 266, 273

Davenport, J. R. A., West, A. A., Matthiesen, C. K., Schmieding, M., Kobelski, A. 2006, PASP, 118, 1679

Dehnen, W., Binney, J. J. 1998, MNRAS, 298, 387 (DB98)

Feast, M. W., Whitelock, P. A. 1997, MNRAS, 291, 683

Fuchs, B., Dettbarn, C., Jahreiß, H., Wielen, R. 2001, ASP Conf. Ser., Vol. 228, 235

Fuchs, B., Wielen, R. 1987, The Galaxy, G. Gilmore, B. Carswell (eds.), Reidel, 375

Fukugita, M., Ichikawa, T., Gunn, J.E., Doi, M., Shimasaku, K., & Schneider, D.P. 1996, AJ, 111, 1748

Gilmore G. 1989, The Milky Way as a galaxy, G. Gilmore, I. King, P. van der Kruit (eds.), Geneva: Swiss Soc. Astroph. Astron, 143

Gliese, W. 1957, Astr. Rechen-Inst. Heidelberg, Mitt. A, No. 8

Gunn, J.E., et al. 1998, AJ, 116, 3040

Gunn, J.E., et al. 2006, AJ, 131, 2332

Harris, W. E. 1996, AJ, 112, 1487

Hogg, D.W., Finkbeiner, D.P., Schlegel, D.J., & Gunn, J.E. 2001, AJ, 122, 2129

Holmberg, J., Nordström, B., Andersen, J. 2007, A&A, 475, 519

Ivezić, Ž., et al. 2004, AN, 325, 583

Ivezić, Ž., Bond, N., Jurić, M., Munn, J. A., Lupton, R. H. et al. 2005, ASP Conf. Ser., 338, 201

Jahreiß, H., Wielen, R. 1997, HIPPARCOS'97, B. Battrick, M.A.C. Perryman, P.L. Bernacca (eds.), Noordwijk: ESA SP-402, 675

Jurić, M., Ivezić, Ž., Brooks, A., Lupton, R. H., Schlegel, D. et al. 2008, ApJ, 673, 864

Kent, S. M., de Zeeuw, T. 1991, AJ, 102, 1994

Klement, R., Fuchs, B., Rix, H.-W. 2008, ApJ, 685, 261

Luyten, W. J. 1939, Publ. Obs. Minnesota II, 123

Lee, Y. S., Beers, T. C., Sivarani, T., Allende Prieto, C., Koesterke, L., Wilhelm, R., et al. 2008a, 136, 2022

Lee, Y. S., Beers, T. C., Sivarani, T., Johnson, J. A., An, D., Wilhelm, R., et al. 2008b, AJ, 136, 2050

Monet, D. G., Levine, S. E., Canzian, B., Ables, H. D., Bird, A. et al. 2003, AJ, 125, 984

Munn, J. A., Monet, D. G., Levine, S. E., Canzian, B., Pier, J. R. et al. 2004, AJ, 127, 3034

Nordström, B., Mayor, M., Andersen, J., Homberg, J., Pont, F. et al. 2004, A&A, 418, 989

Pier, J.R., Munn, J.A., Hindsley, R.B., Hennessy, G.S., Kent, S.M., Lupton, R.H., & Ivezić, Ž. 2003, AJ, 125, 1559

Siebert, A., Bienaymé, O., Binney, J., Bland-Hawthorn,J., Campbell, R. et al. 2008, MNRAS, in press

Smith, J.A., et al. 2002, AJ, 123, 2121

Spitzer, L., Schwarzschild, M. 1951, ApJ, 114, 385

Steinmetz, M., Zwitter, T., Siebert, A., Watson, F. G., Freeman, K. C. et al. 2006, AJ, 132, 1645

Stoughton, C., et al. 2002, AJ, 123, 485

Tucker, D. L., Kent, S., Richmond, M. W., Annis, J., Smith, J. A. et al. 2006, AN, 327, 821

Veltz, L., Bienayme, O., Freeman, K. C., Binney, J., Bland-Hawthorne, J. et al. 2008, (arXiv:0801.2120)

West, A. A., Walkowicz, L. M., Hawley, S. L. 2005, PASP, 117, 706

West, A. A., Hawley, S. L., Bochanski, J. J., Covey, K. R., Reid, I. N. 2008, AJ, 135, 785

Yanny, B., et al. 2008, AJ, submitted

York, D.G., et al. 2000, AJ, 120, 1579

Zwitter, T., Siebert, A., Munari, U., Freeman, K.C., Siviero, A. et al. 2008, AJ, 136, 421

This 2-column preprint was prepared with the AAS LaTeX macros v5.2.

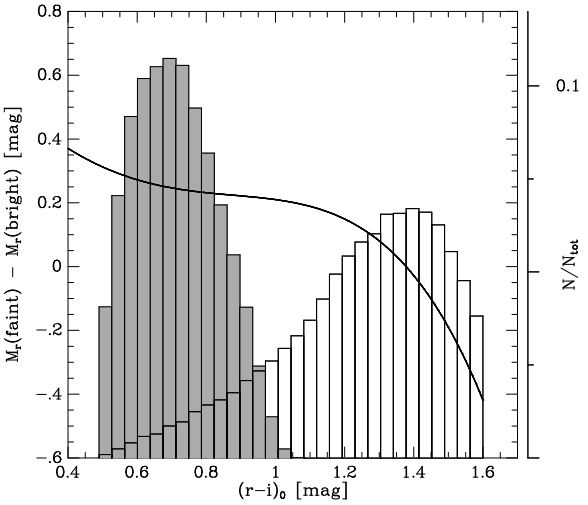

Fig. 1.— Difference between the faint and the bright normalization of the absolute magnitude M_r-color relation by Jurić et al. (2008), as a function of $(r-i)_0$ color (solid line). Underlaid as white histogram is the frequency distribution of the M stars in the distance bin closest to the Galactic midplane, while the grey histogram shows the corresponding distribution in the most distant bin. Both histograms are normalized to unity (scale on the right).

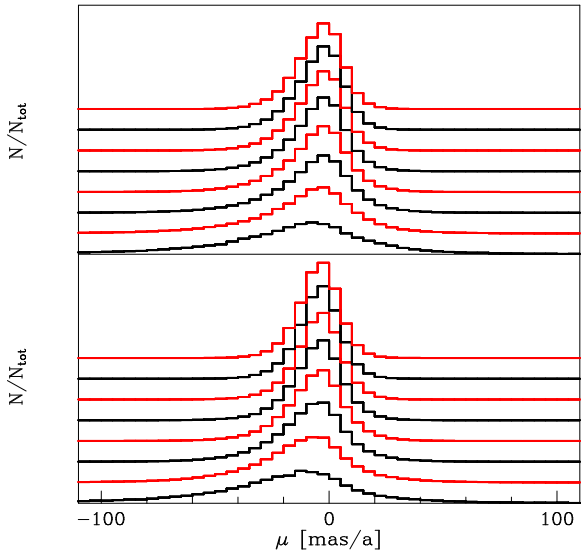

Fig. 2.— Frequency distributions of the proper motions in right ascension (top panel) and declination (bottom panel) for the stars in each of the eight counting volumes. The histograms are each normalized to unity and shifted relative to each other so that the Z-slice closest to the Galactic midplane appears as lowest and the most distant Z-slice at the top.

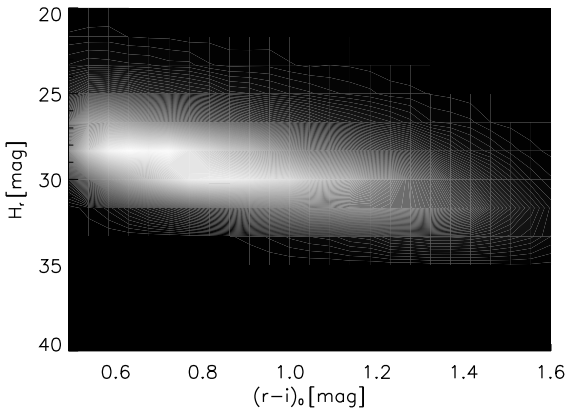

Fig. 3.— Greyscale diagram of the frequency distribution of the reduced proper motions of the selected M stars versus their $(r-i)_0$ colors. The distribution is shown on a linear scale, coded from black to white.

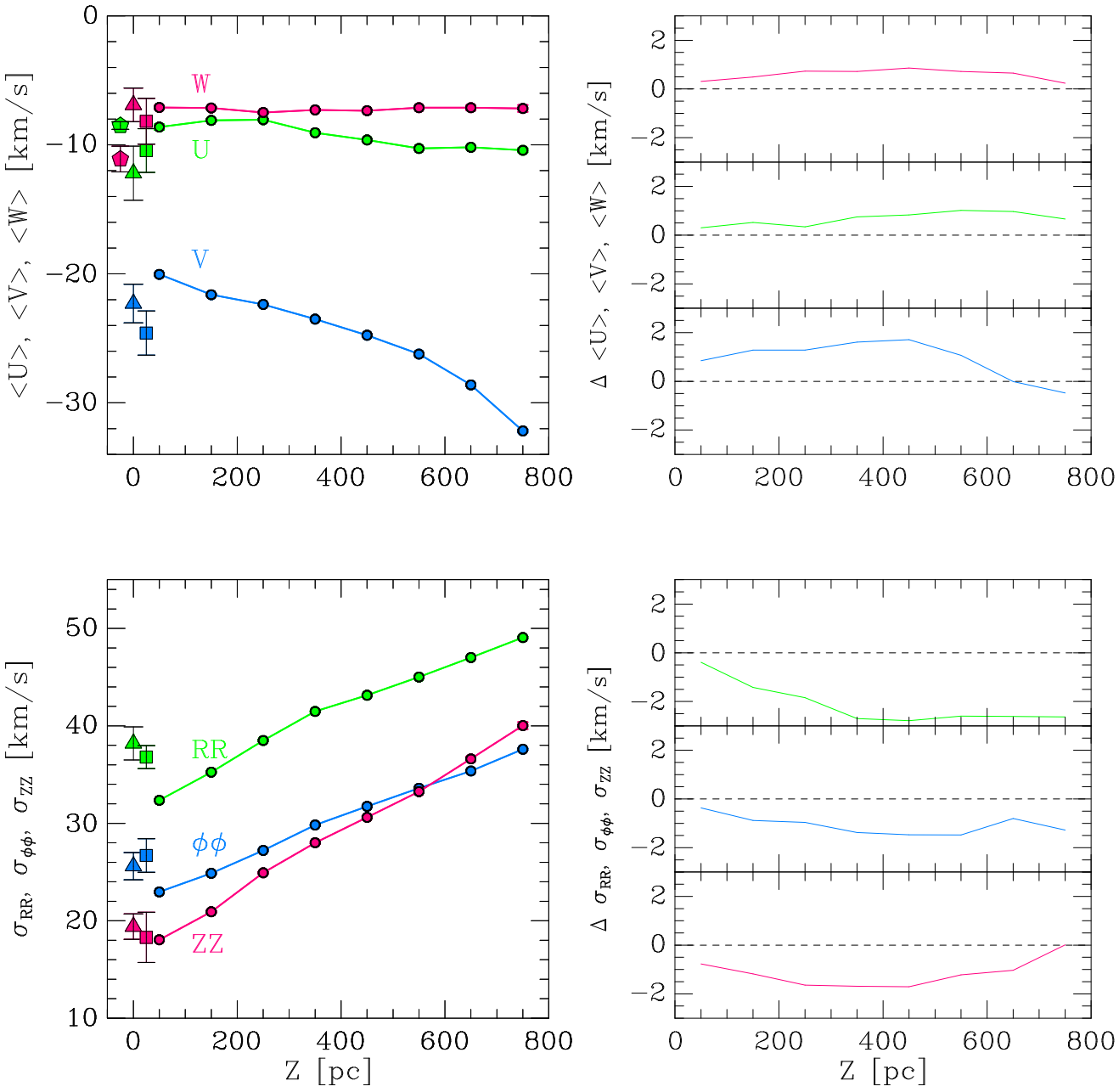

Fig. 6.— Top left panel: The first moments $\langle U \rangle$, $\langle V \rangle$, and $\langle W \rangle$ as a function of height Z above the Galactic midplane (solid dots), as determined in this work. Solar neighborhood data (triangles) and the results of Dehnen & Binney (1998) (squares) and Veltz et al. (2008) (pentagons) are indicated at $Z = 0$. Bottom left panel: The velocity dispersions σ_{RR}, $\sigma_{\phi\phi}$, and σ_{ZZ} as a function of height Z above the Galactic midplane (solid dots) as determined in this work. The solar neighborhood data (triangles) and results of Dehnen & Binney (1998) (squares) are indicated at $Z = 0$. Top right panel: Differences of the mean velocities $\langle U \rangle$, $\langle V \rangle$, and $\langle W \rangle$ (color coded as in the left panel) determined with the faint normalization of the absolute magnitudes minus the mean velocities determined with the bright normalization (Jurić et al. 2008). Bottom right panel: Same as upper panel, but for the velocity dispersions σ_{RR}, $\sigma_{\phi\phi}$, and σ_{ZZ}. The right panels indicate that the systematic errors of our results are of the order of 2 to 3 km/s.

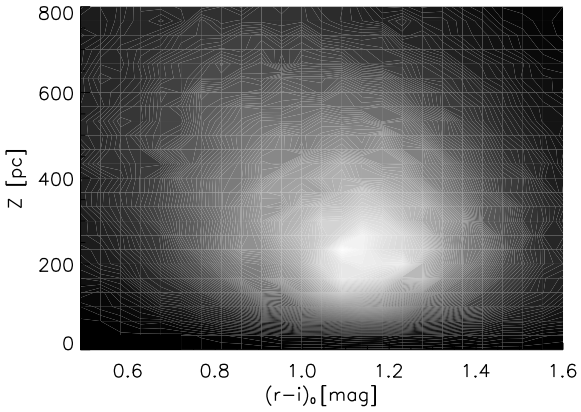

Fig. 4.— Greyscale illustration of the distribution of the M stars in our sample as function of height above the Galactic midplane and $(r-i)_0$ color. The density is shown on a linear scale, coded from black to white.

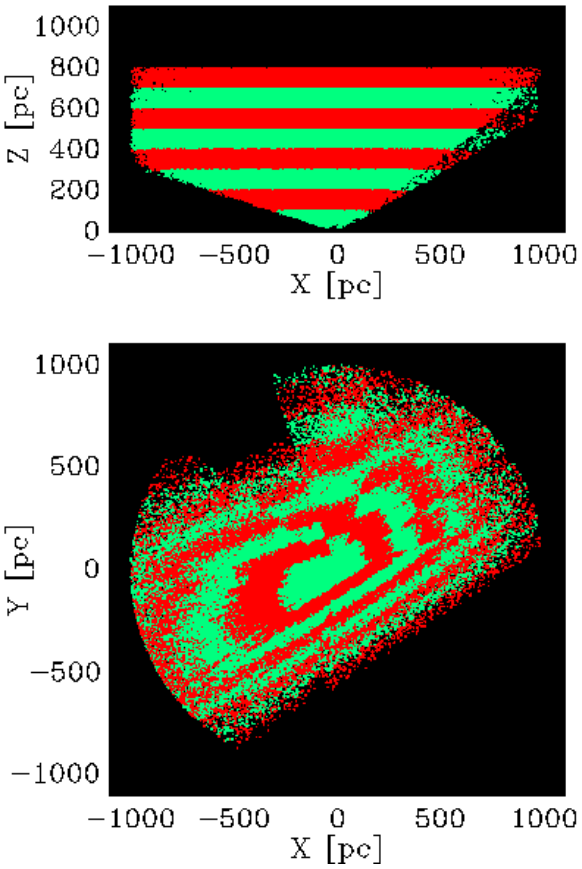

Fig. 5.— Spatial distribution of the sample stars. The upper panel shows the distribution in Galactocentric radius X and height above the Galactic midplane Z. The conical distribution reflects the geometry of the survey. The lower panel illustrates the projection onto the Galactic plane. The layers are shown stacked opaquely onto each other viewed from below the Galactic midplane.

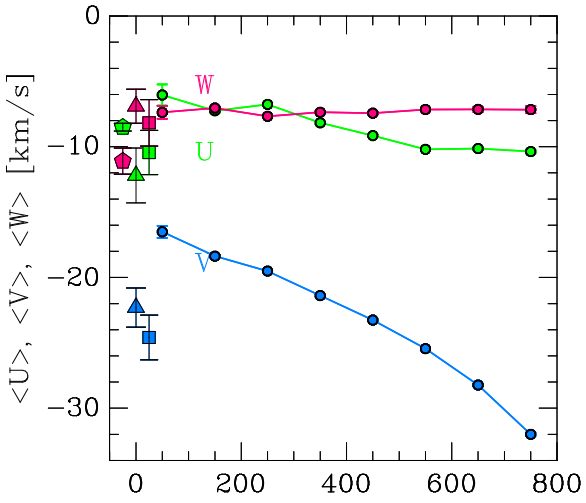

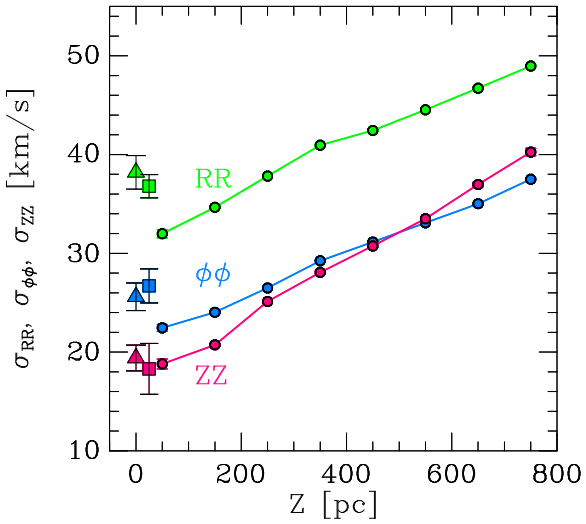

Fig. 7.— Same as Fig. 6, but using only stars with colors $0.49 \leq (r-i)_0 \leq 0.9$. The systematic errors of our results are of the order of 2 to 3 km/s.

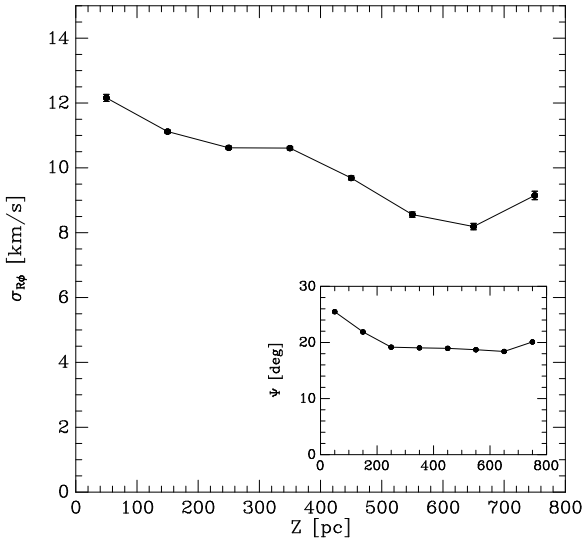

Fig. 8.— The mixed element $-\sigma_{R\phi}$ of the velocity dispersion tensor as a function of height above the Galactic midplane Z. The inset shows the vertex deviation of the velocity ellipsoid.

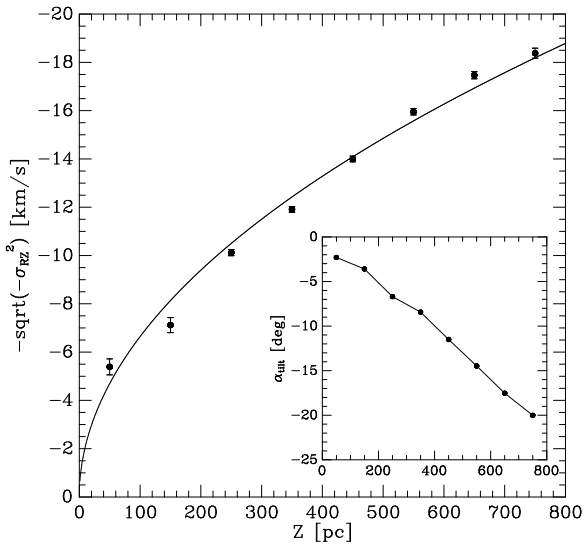

Fig. 9.— The mixed element $-\sqrt{\sigma_{RZ}^2}$ of the velocity dispersion tensor as a function of height above the Galactic midplane Z. The solid line line is a polynomial fit. The inset shows the apparent tilting angle of the velocity ellipsoid.